Present-Day Stress Orientation in the Molasse Basin

John Reinecker[a*], Mark Tingay[b], Birgit Müller[c,d] and Oliver Heidbach[d,e]

[a]*Institute for Geosciences, University of Tübingen, Sigwartstr. 10, 72076 Tübingen, Germany*
[b]*Department of Applied Geology, Curtin University of Technology, Perth, 6845 WA.*
[c]*Heidelberg Academy of Sciences and Humanities, Karlstr.4, 9117 Heidelberg, Germany*
[d]*Geophysical Institute, University of Karlsruhe, Hertzstr.16, 76187 Karlsruhe, Germany*
[e]*now at German Research Centre for Geosciences, Telegrafenberg, 14473 Potsdam, Germany*

Abstract

The present-day state of stress in Western Europe is considered to be controlled by forces acting at the plate boundaries. It is assumed that the Alpine orogen only influence the regional pattern of present-day stress in Western Europe within the Alps themselves. We examine the present-day maximum horizontal stress orientation in the Molasse Basin in the Alpine foreland in order to investigate the possible influence of the Alps on the far-field stress pattern of Western Europe. Four-arm caliper and image logs were analysed in 137 wells, in which a total of 1348 borehole breakouts and 59 drilling-induced fractures were observed in 98 wells in the German Molasse Basin. The borehole breakouts and drilling-induced fractures reveal that stress orientations are highly consistent within the Molasse Basin and that the present-day maximum horizontal stress orientation rotates from N-S in southeast Germany (002ºN ± 19º) to approximately NNW-SSE in southwest Germany and the Swiss Molasse Basin (150ºN ± 24º). The present-day maximum horizontal stress orientation in the Molasse Basin is broadly perpendicular to the strike of the Alpine front, indicating that the stress pattern is probably controlled by gravitational potential energy of Alpine topography rather than by plate boundary forces. The present-day maximum horizontal stress orientations determined herein have important implications for the production of hydrocarbons and geothermal energy in the German Molasse Basin, in

particular that hydraulically-induced fractures are likely to propagate N-S and that wells deviated to the north or south may have reduced wellbore instability problems.

Keywords: stress field; borehole breakouts; drilling induced fractures; tectonics; Molasse Basin

1. Introduction

The present-day stress field of Western Europe is considered to be primarily controlled by resistance forces generated by Eurasia-Africa plate collision and ridge-push forces exerted by the mid-Atlantic spreading centre (Müller et al., 1992; Zoback, 1992; Grünthal and Stromeyer, 1986). The first-order control of the Europe-Africa boundary and the mid-Atlantic Ridge on the stress field in Western Europe is supported by the predominantly NW-SE present-day maximum horizontal stress (S_H) orientation (mean S_H orientation of 144°N; Müller et al., 1992; Heidbach et al., 2007), the observation that S_H is sub-parallel to relative plate motion (Müller et al., 1992; Richardson, 1992) and by means of plate-scale finite element modelling of the stress field (Grünthal and Stromeyer, 1992; Gölke and Coblentz, 1996). However, these models downplay the influence of intraplate sources of stress, particularly the Alpine orogen, on the stress field in Western Europe.

The plate boundary driven models of stress in Europe have been used to suggest that forces generated by the Alpine orogen have only a negligible impact on the Western European stress field, resulting only in extensional stresses within the Alps themselves (Zoback, 1992; Gölke and Coblentz, 1996). However, the Alpine orogen has had a dominant and widespread far-field influence on the Cenozoic tectonics in Western Europe (Cloetingh, 1986; Ziegler, 1987). Illies and Greiner (1978) postulate that the S_H orientations are

51 approximately perpendicular to the isobases of Holocene uplift in the Rhine Graben.
52 Stresses generated by the Alpine orogen are hypothesised to have been transmitted over
53 1500 kilometres from the Alps, resulting in uplift and inversion in numerous areas such as
54 the UK and southern North Sea (Cloetingh, 1986; Ziegler 1990; Hillis et al., 2008).
55 Furthermore, recent compilations of S_H orientations reveal that the stress pattern in
56 Western Europe is less homogeneous than previously assumed. The wave-lengths of the
57 stress pattern range from tens to hundreds of kilometres (Müller et al., 1997; Tingay et al.,
58 2006; Heidbach et al., 2007; Heidbach et al., this issue). These second- and third-order
59 stress pattern indicate that localised intraplate sources of stress, such as gravitational
60 potential energy of the elevated Alpine orogen as well as lateral density and strength
61 contrasts can locally overrule the far-field stress contribution in Western Europe and
62 determine the S_H orientations (Tingay et al., 2006; Heidbach et al., 2007).

63 The new data from the Molasse Basin, immediately adjacent to the Alps, provides an
64 opportunity to better understand the relative influence of the Alpine orogen on the
65 European stress pattern. The plate boundary driven models suggest that the Alpine orogen
66 generates only minor gravitational forces localised within the Alps and that a NW-SE to
67 NNW-SSE S_H pattern should be observed throughout the Alpine foreland (and most of
68 Germany and France; Gölke and Coblentz, 1996). However, the S_H orientation would be
69 expected to be roughly perpendicular to the Alpine front (rotating from N-S in southeast
70 Germany to approximately NNW-SSE in southwest Germany) if gravitational and
71 collisional resistance forces generated by the Alps are significantly influencing the stress
72 pattern in the Alpine foreland.

73 In this study we conduct the first regional investigation of the present-day S_H orientation in
74 the German Molasse Basin. We use borehole breakouts interpreted from four-arm caliper

and image log data from hydrocarbon and geothermal wells. We discuss localised stress variations, the stress regime, and the sources of the stress field.

2. Geology and tectonic evolution

The Molasse Basin, located immediately north of the Alps, is considered a classical peripheral foreland basin. It extends over a lateral distance of approximately 1000 km from Lake Geneva in the west to Lower Austria in the east and has a present-day maximum width of 130 km in Bavaria, SE Germany (Fig. 1). The basin has a typically asymmetric cross-section with its deepest part along the Alpine thrust front in SE Bavaria. The Molasse Basin is filled with up to 5000 m of predominantly Late Eocene to Late Miocene sediments of different facies, comprising fluvial fans to deep-marine sandstones, marls and clays (Fig. 1; see Bachmann et al., 1982; Bachmann et al., 1987, and Kuhlemann and Kempf, 2002 for details on basin evolution). The Tertiary strata are underlain by 500-1000 m of Mesozoic shelf sediments, local Permo-Carboniferous troughs containing unknown thicknesses of clastics, and the Variscan basement.

Basin formation and sedimentation is primarily due to the northward thrusting and isostatic uplift of Alpine nappes and associated down bending of the European plate. At smaller scales, basin formation has been influenced by the inherited structures of the pre-Tertiary basement (Bachmann et al., 1987). Subsidence of the Molasse Basin was initiated and controlled by Alpine nappe tectonics in the south and resulted in formation of E-W striking normal faults that are currently inactive. Over the course of basin evolution, Alpine nappes were thrust northward by up to 50 km onto the Molasse sediments (Bachmann et al., 1987). During thrusting, Molasse sediments in the south became subsequently incorporated into Alpine nappe tectonics (‘Subalpine Molasse’), in contrast to the more or less undisturbed

99 'Autochthonous Molasse' in the north and below the Subalpine Molasse. Betz and Wendt
100 (1983) and Brink et al. (1992) describe broad anticlines in the Swiss Molasse Basin, which
101 are very rare in the German part, probably because of the absence of preferred décollement
102 horizons like the Muschelkalk evaporites in Switzerland. Compressive stresses resulting in
103 these folds are believed to result form the northward propagation of Alpine nappes and the
104 topography of the orogen (Illies and Greiner, 1978).

105

106 **3. Stress orientation from borehole breakout and drilling-induced fracture analysis**

107 The S_H orientation in the Molasse Basin was determined herein from borehole breakouts
108 (BO) and drilling-induced fractures (DIF). Breakouts are stress-induced enlargements of
109 the wellbore cross-section (Bell and Gough, 1979). When a wellbore is drilled, the material
110 removed from the subsurface is no longer supporting the surrounding rock. As a result, the
111 stresses become concentrated in the surrounding rock (i.e. the wellbore wall). Borehole
112 breakout occurs when stresses around the borehole exceed the compressive strength of the
113 borehole wall (Zoback et al., 1985; Bell, 1990). The enlargement of the wellbore is caused
114 by the development of intersecting conjugate shear planes that cause pieces of the borehole
115 wall to spall off (Zoback et al., 1985). The stress concentration around a vertical borehole
116 is greatest in the direction of the minimum horizontal stress (S_h). Hence, the long axes of
117 borehole breakouts are oriented approximately perpendicular to the S_H orientation. DIF's
118 are created when the stresses concentrated around a borehole exceed the tensile strength of
119 the wellbore wall (Aadnoy, 1990). DIF's typically develop as narrow sharply defined
120 features that are sub-parallel or slightly inclined to the borehole axis in vertical wells. The
121 stress concentration around a vertical borehole is at a minimum in the S_H direction. Hence,
122 DIF's develop approximately parallel to the S_H orientation (Aadnoy and Bell, 1998).

Borehole breakouts are interpreted in this study from the analysis of four-arm caliper log data from 132 wells (Table 1). The interpretation of borehole breakouts from caliper log data is conducted using the standard breakout interpretation methodology, with all breakouts being manually interpreted (Bell and Gough, 1979; Plumb and Hickman, 1985; Zoback et al., 1985; Reinecker et al., 2003). Image logs are available from five wells, from which we are able to visually identify DIF's as well as borehole breakout (Tingay et al., 2008). All but 15 wells in the study are sub-vertical and no stress-induced features were included from wells with deviations greater than 5° from vertical if the hole elongation azimuth was within 15° of the hole deviation direction. The average S_H orientation and standard deviation of the stress-induced features observed in each well are calculated using circular statistical analysis following Mardia (1972). The average S_H orientations for each well are quality-ranked according to the updated World Stress Map criteria and available in the World Stress Map 2008 database release (Heidbach et al., 2008; Heidbach et al., this issue).

4. Stress field in the German Molasse Basin

Approximately 167 kilometres of four-arm caliper and 2.5 kilometres of image log data are analysed from the German Molasse Basin, revealing a total of 1348 breakouts and 59 DIF's in 98 wells (Table 1). S_H orientations from 67 wells are ranked A-C quality and used in the analysis herein (Table 1; Fig. 2; Fig. 3). The borehole breakouts and DIF's interpreted herein indicate a highly uniform north-south S_H orientation (average 002ºN with standard deviation of 19.2º; Fig. 2C) within the Molasse Basin and below in the pre-Tertiary basement. Some wells show perturbed S_H orientations from the dominant N-S orientation but without any regional trend within the Molasse Basin. Localized stress

147 perturbations can be caused by proximity to nearby faults or other structures and in most
148 cases the wells with possible stress rotations are of low quality (see discussion below). No
149 significant rotation of S_H orientation with depth is found from this analysis (Fig. 3A,C).
150 The high ratio between breakouts and well log lengths (with values up to 65 %; Fig. 3B,D)
151 show that horizontal differential stresses ($S_{HD} = S_H - S_h$) are sufficiently high to create
152 breakouts within large volumes of the Molasse Basin.

153 The N-S S_H orientation observed in most of the German Molasse Basin is consistent with
154 the S_H orientation estimated from pressure solution of pebbles in Molasse Basin sequences
155 (Schrader, 1988). S_H orientations estimated from earthquake focal mechanisms below the
156 western part of the German Molasse Basin show the same N-S compression, suggesting
157 that the regional S_H orientations do not vary significantly at crustal scale (Fig.4; Müller et
158 al., 1997; Kastrup et al., 2004).

159

160 **5. Discussion**

161 *Localised variations of S_H orientation*

162 Most of the analysed wells are drilled by oil and gas exploration companies. Within the
163 German Molasse Basin structural traps are commonly characterised by partly sealing E-W
164 to NE-SW striking synthetic and antithetic normal faults (Brink et al. 1992). Therefore the
165 proximity of these structures is quite likely to locally perturb the stress field in some
166 locations.

167 Localised variations of up to 90º from the regional N-S S_H trend are observed in Illmensee
168 5 and 8, Mönchsrot 26, Tacherting 1b, Aitingen 4a, Höhenrain A5, Schmidhausen A3,
169 Inzenham-West 14, Breitbrunn C10, Schnaitsee 7, Vorderriss 1, and Hindelang 3L (all of

A-C quality; Fig. 2A,B; Table 1). All, but the latter two are drilled within the foreland Molasse Basin.

The observed breakout zones in wells Hindelang 3L and Vorderriss 1 are located within the Alpine thrust belt (Fig. 2A and 3A; Table 1). In the lowest part Hindelang 3L has reached the allochthonous (folded) Molasse. The S_H orientation is consistently NW-SE in these two wells, but with a high standard deviation of 22°. The origin of this NW-SE S_H orientation is unknown. However, the high standard deviation of the S_H orientations may reflect local perturbations due to the complex structure of the penetrated Alpine nappe stack. From modelling studies we can exclude an influence of the sharp topographic relief in intramontane regions on S_H orientation at depth greater than 500 m (Engelder, 1993). Lithostatic overpressures, as observed in Hindelang 3L, may indicate either rapid sedimentary or tectonic loading, or a high degree of shearing. The latter is believed to be the case for Hindelang 3L and may be accompanied by additional lateral stress (Müller and Nieberding, 1995, 1996). Here the breakouts occur in the zone of overpressure, but due to lack of data we can not exclude breakouts to be present in zones of normal pressure. In contrast Vorderriss 1 does not show overpressures. However, the quality of sealing, which depends on the structural geology and lithology, seems critical to encounter overpressures (Müller and Nieberding, 1995, 1996). So up to now we can not explain the NW-SE S_H orientation observed in these two wells.

The field Illmensee is located in the westernmost part of the German Molasse Basin. The local stress field there is the least constrained in the study area. Nearby wells show very different S_H orientations. Illmensee 6 and 7 fit in the regional N-S trend of the S_H orientation. Illmensee 8 and 5 instead indicate E-W and NE-SW S_H orientations, respectively (Figure 2A,B; Table 1). However, further to the east a clear N-S S_H orientation is observed in the wells Ravensburg 1, Grünlingen 1, and Frohnhofen 16 (Fig. 2A).

195 The wells Mönchsrot 26 and Tacherting 1b contain breakouts indicating approximately E-
196 W S_H orientations at relatively shallow depths (<1900 m), although N-S S_H orientations are
197 observed in deeper sequences of these and nearby wells (Fig. 2A,B and 3A; Table 1).

198 The analysed log intervals from the wells Schmidhausen A3, Inzenham-West 14,
199 Höhenrain A5, and the uppermost section of Breitbrunn C10 are all short, very shallow
200 (<1000 m), and indicate NE-SW S_H orientations (Figure 2A,B; Table 1). Aitingen 4a is the
201 only well showing NW-SE S_H orientation within the German Molasse Basin (Figure 2A;
202 Table 1). In all cases we are not able to address stratigraphic correlation of the abnormal
203 stress orientations, but nearby wells clearly indicate N-S S_H orientation with a high quality
204 at comparable depths suggesting that active faults at depth probably locally perturb the S_H
205 orientation.

206 Schnaitsee 7 is the only well where we have evidence for abrupt rotation of the S_H
207 orientation from N-S within the Molasse sequences to NW-SE in the underlying Mesozoic
208 strata. The NW-SE S_H orientation is of only D-quality and should therefore not be over
209 interpreted.

210 We can not exclude the possibility that these abnormal S_H orientations may be artefacts
211 resulting from large DIF's being incorrectly interpreted as breakouts on four-arm caliper
212 log data. An accurate distinction between breakouts and large DIF's can only be made
213 from high resolution image logs, which are rarely run in the Molasse Basin during the main
214 period of exploration activity between 1970 and 1990.

215

216 *Estimates of the relative state of stress in the Molasse Basin*

217 No data was available for this study to directly examine stress magnitudes. However, it is
218 possible to speculate on the state of stress in the German Molasse Basin based on the stress

pattern and further details of the wellbore failure observations. Over 1300 breakouts are interpreted in this study and breakouts were often observed to have large angular widths (>60º), high eccentricities (>50% more than bit size) and occur at shallow depths (at <600 m depth in 27 wells, with some breakout observed at less than 100 m depth).

Breakouts and DIF's require high horizontal stresses and, typically, horizontal stress differences to develop (Engelder, 1993; Haimson and Herrick, 1989). Breakout width and eccentricity have been used to give an indication on the magnitude of horizontal differential stress (Zoback et al., 1985; Haimson and Herrick, 1989). Laboratory studies suggest that the width of breakouts in vertical wells is proportional to the ratio of the two horizontal principal stresses S_H/S_h and can help constrain the in-situ stress tensor (Zoback et al., 1985; Barton et al., 1988; Zajak and Stock, 1997). Hence, breakouts that exhibit high angular widths can be used as a rough proxy for the value of S_{HD} (Zoback et al., 1985; Haimson and Herrick, 1989; Engelder, 1993). The high angular widths and eccentricities of breakouts observed in this study suggest that S_{HD} values are high in the Molasse Basin.

The four-arm caliper log datasets examined herein contain, rather unusually, a significant number of logging runs at very shallow depth, with 43 wells containing caliper log at depths shallower than 500 m. Furthermore, the shallow caliper log data examined herein revealed that breakouts in the German Molasse Basin occur at very shallow depths, with the shallowest breakout observed at just 67 m below the surface. Breakouts are rarely observed at such shallow depths, particularly in petroleum wells in which the pressure of the drilling mud improves the stability of the wellbore. In general, the S_{HD} in shallow sedimentary sequences are typically too low to induce failure. Furthermore, shallow sediments are unconsolidated and weak and thus unable to transmit high magnitudes of shear stress. Hence, the unusual observation of breakouts at shallow depths suggests that

243 the horizontal stress magnitudes (or, at least S_H magnitude) are quite high in the Molasse
244 Basin.

245 The occurrence of small-scale stress perturbations, such as those discussed in the previous
246 section, is frequently considered to indicate that horizontal stress magnitudes are relatively
247 similar and/or that local intra-basinal sources of stress dominate over far-field sources
248 (Sonder, 1990; Bell, 1996; Tingay et al., 2006). However, the inference of similar S_H and
249 S_h magnitudes due to the presence of small-scale stress perturbations is inconsistent with
250 the observations of wellbore failure at low depth discussed above.

251 The majority of stress regimes inferred from earthquake focal mechanisms, recent
252 structural styles in the region, and observations of thrust deformation in the lignite mine of
253 Peissenberg (Heissbauer, 1975; Illies and Greiner, 1978) indicate that a strike-slip or thrust
254 faulting stress regime is most likely present in the Molasse Basin (Fig. 4). Therefore, we
255 speculate that the characteristics of wellbore failure, combined with the observed recent
256 structural and fault styles, indicate that a strike-slip ($S_H>S_v>S_h$) or thrust ($S_H>S_h>S_v$)
257 faulting stress regime presently exists in the German Molasse Basin.

258

259 *Sources of the North Alpine foreland stress field*

260 Plate boundary forces resulting from northward motion and counter clockwise rotation of
261 Adria relative to stable Europe, together with push from the north Atlantic mid ocean
262 ridge, are commonly suggested to control the stress field in central and western Europe
263 (e.g. Müller et al., 1992). On the other hand, stresses resulting from buoyancy forces
264 associated with elevated topography and related thickened crust of the Alps may also
265 significantly contribute to the stress pattern in the north Alpine foreland.

266 The general pattern of S_H orientations within the Molasse Basin is perpendicular to the
267 strike of the Alpine front in the near vicinity north of the Alps between Lake Geneva and
268 Salzburg (Fig. 2A,B and 4; Kastrup et al., 2004). WNW-ESE S_H orientations found in the
269 eastern Swiss Molasse Basin and the eastern Jura Mountains (Becker, 2000) are controlled
270 by the influence of the Black Forest Massif. Further to the east (between Salzburg and
271 Vienna), the stress pattern seems to be regionally perturbed by the Bohemian Massif acting
272 as a rigid indenter (Reinecker and Lenhardt, 1999).

273 S_H orientations change with depth in the western Swiss Molasse Basin due to Mesozoic
274 evaporite layers below the Molasse Basin, which are acting as décollement horizons (e.g.
275 Brereton and Müller, 1991). However, no such evaporitic layers are known to occur in the
276 German Molasse Basin and no systematic stress rotations with depth are observed in the
277 German Alpine foreland. The well Bromberg 1 (Fig. 3A) is a nice example for a
278 continuous stress profile from the Tertiary Molasse Basin into the underlying Mesozoic
279 strata indicating N-S S_H orientation down to 4.7 km depth. The observed overpressures in
280 this well have no effect on the S_H orientation (Müller and Nieberding, 1996). Also the
281 wells Grambach 1 and Bad Waldsee 2 provide further evidence that S_H orientations are
282 generally N-S in the German Molasse Basin and below to depths of 6 km (Fig. 3A,C). S_H
283 orientations from earthquake focal mechanisms in the western German Molasse Basin
284 support this hypothesis (Fig. 4).

285 The observation that S_H is oriented perpendicular to the Alpine front, and not restricted to
286 the Molasse sediment sequence, indicates that the present-day stress pattern in the foreland
287 is probably controlled by the gravitational potential energy generated by Alpine
288 topography. Furthermore, the N-S S_H orientation is observed over 100 km from the Alpine
289 front, suggesting that topographic stresses can be transmitted larger distances away from
290 mountain ranges (Fig. 2, Fig.4).

In-situ stresses at any given point are the combined result of far-field and local sources of stress, and thus, stress orientations should typically not be considered to result from only one source of stress (Sonder, 1990; Tingay et al., 2006). Hence, although gravitational forces appear to be the dominant control on regional stress orientations in the Molasse Basin, the stress field may still be influenced by plate-boundary forces, albeit to a lesser degree.

Implications for hydrocarbon and geothermal production

The numerous wide and highly eccentric breakouts observed in this study suggest that mechanical wellbore instability may be a significant issue for the drilling of hydrocarbon and geothermal wells in the Molasse Basin. The number of breakouts, and thus mechanical instability of the borehole, can be reduced by raising the mud weight and/or altering borehole deviation and azimuth in order to lower the circumferential stress acting on the wellbore (Aadnoy and Chenevery, 1987; Moos and Peska, 1998; Aadnoy, 2003). It is generally considered that vertical boreholes are least stable in strike-slip faulting stress regimes, while wells deviated towards the S_h direction are least stable in thrust faulting stress regimes (Mastin, 1988; Peska and Zoback, 1995). Hence, in the absence of detailed stress magnitudes, we predict that wells deviated towards S_H in the Molasse Basin (i.e. N-S in southeast Germany and NNW-SSE in southwest Germany) are likely to have the lowest absolute stress magnitudes and differential stresses acting upon them and, thus be more mechanically stable.

The present-day state of stress is also a key influence on fluid flow through both natural and hydraulically-induced fractures and is thus of key significance for geothermal and petroleum production in the Molasse Basin. Hydraulically-induced fractures open against

315 the minimum principal stress (typically S_h; Hubbert & Willis, 1957). Hence, hydraulic
316 fractures induced in the Molasse Basin would be expected to strike parallel to S_H (N-S to
317 NNW-SSE) if a strike-slip stress regime is present, or to be sub-horizontal in a thrust
318 faulting stress regime. Natural fractures that are most suitably oriented for tensile or shear
319 failure in the present-day stress tensor, typically those fractures striking parallel to or
320 within 30º of the maximum principal stress respectively, are observed to transmit the
321 greatest volumes of fluids in many fractured rocks (Barton et al., 1995; Sibson, 1996).
322 Hence, any engineered geothermal production planned in fractured reservoirs in the
323 Molasse Basin should target natural fractures that are optimally oriented for failure in the
324 present-day stress tensor, namely sub-vertical fractures that strike between NNW and NNE
325 in a strike-slip stress regime, or fractures that are sub-horizontal or dipping approximately
326 30 º towards the north or south in a thrust faulting stress regime.

327

328 *Implications for other foreland basins*

329 The hypothesis that topographic body forces from the Alps may influence the far-field
330 intraplate stress pattern is largely inconsistent with generally accepted theory that large-
331 scale stress patterns are controlled by plate boundary forces (Zoback, 1992; Richardson,
332 1992; Zoback and Mooney, 2003). However, it is interesting to note that similar stress
333 patterns have been observed from borehole breakout analysis in other foreland basins.
334 Similar regional stress field analysis has also been conducted in the Alberta and Neuquén
335 Basins, foreland basins of the Rockies and Andes respectively, and both reveal S_H
336 orientations that are consistently perpendicular to the strike of the topographic front (Bell,
337 1996; Guzmán et al., 2007, Guzmán and Cristallini, 2009). The S_H orientations observed in
338 the Alberta and Neuquén Basins, and in the southwest part of the Molasse Basin, are
339 consistent with absolute plate motion and thus have been used to suggest that plate

boundary forces, rather than gravitational forces, control the S_H orientation in these foreland areas (Richardson, 1992; Zoback, 1992; Gölke and Coblentz, 1996; Guzmán et al., 2007; Guzmán and Cristallini, 2009). However, the strike of the topographic front is largely perpendicular to the direction of relative plate motion in the Alberta, Neuquén, Cuya and southwest Molasse Basins, and thus both topographic body forces and plate boundary forces may be expected to yield similar S_H orientations. In contrast, the section of the Molasse Basin in southeast Germany provides an opportunity to distinguish between the stress patterns generated by intraplate topographic body forces from that generated by plate boundary forces. Therefore, we suggest that the present-day S_H orientations observed in the Alberta, Cuya and Neuquén Basins may also predominantly reflect intraplate topographic body forces, rather than stresses generated by plate boundary forces. Furthermore, we predict that present-day S_H orientations are likely to be perpendicular to the topographic front in other foreland basins, particularly those that are mechanically detached from the basement.

6. Conclusions

The S_H orientations observed in this study yield the first regional understanding of the stress pattern in the German Molasse Basin. The mean S_H orientation rotates ~30° counterclock-wise from N-S in southeast Germany to NNW-SSW in southwest Germany and the Swiss Molasse Basin and, quite significantly, shows a clear correlation with the strike of the Alpine front (Fig. 2; Fig. 4). We suggest that the gravitational potential energy generated by Alpine topography is the dominant source of stress in the Molasse Basin. Furthermore, N-S S_H orientations are observed over 100 km from the Alps into the Northern Alpine foreland, indicating that the Alpine topography may be a significant source of intraplate stresses in Western Europe.

365

366

367 **Acknowledgments**

368 We thank Dr. Thomas Fritzer (LfU, Munich) for his help gathering wellbore data and the
369 Wirtschaftsverband Erdöl- und Erdgasgewinnung for permission to publish the data.
370 Thanks to two anonymous reviewers. Their comments helped clarifying the manuscript.
371 We acknowledge the financial support of the Heidelberg Academy of Sciences and
372 Humanities.

373

374 **References**

375 Aadnoy, B.S., Chenevery, M.E., 1987. Stability of highly inclined boreholes. SPE Drilling
376 Engineering 2, 364-374.

377 Aadnoy, B.S., 1990. Inversion technique to determine the in-situ stress field from
378 fracturing data. Journal of Petroleum Science and Engineering 4, 127-141.

379 Aadnoy, B.S., Bell, J.S., 1998. Classification of drill-induce fractures and their relationship
380 to in-situ stress directions. The Log Analyst 39, 27-42.

381 Aadnoy, B.S., 2003. Introduction to special issue on borehole stability. J. Pet. Sci. and Eng.
382 38, 79-82.

383 Bachmann, G., Dohr, G., Müller, M., 1982. Exploration in a classic thrust and fold belt and
384 its foreland: Bavarian Alps. AAPG Bull. 66, 2529-2542.

385 Bachmann, G., Müller, M., Weggen, K., 1987. Evolution of the Molasse basin (Germany,
386 Switzerland). Tectonophysics 137, 77-92.

387 Barton, C.A., Zoback, M.D., Burns, K.L., 1988. In situ stress orientation and magnitude at
388 the Fenton geothermal site, New Mexico, determined from wellbore breakouts.
389 Geophys. Res. Letters 15, 467-470.

390 Barton, C.A., Zoback, M.D., Moos, D., 1995. Fluid flow along potentially active faults in
391 crystalline rock. Geology 23, 683-686.

392 Bell, J.S., Gough, D.I., 1979. Northeast-southwest compressive stress in Alberta: Evidence
393 from oil wells. Earth and Planetary Science Letters 45, 475-482.

394 Bell, J.S., 1990. Investigating stress regimes in sedimentary basins using information from
395 oil industry wireline logs and drilling records. In: Hurst, A., Lovell, M., Morton, A.

(Eds.), Geological applications of wireline logs. Geol. Soc. London Spec. Publ. 48, 305-325.

Bell, J.S., 1996. Petro Geoscience 1. In situ stresses in sedimentary rocks (part 2): applications of stress measurements. Geoscience Canada 23, 135-153.

Betz, D., Wendt, A., 1983. Neuere Ergebnisse der Aufschluß- und Gewinnungstätigkeit auf Erdöl und Erdgas in Süddeutschland. Bull. Ver. schweiz. Petroleum-Geol. u. Ing. 49 (117), 9-36.

Brereton, R., Müller, B., 1991. European stress: contributions from borehole breakouts. Phil. Trans. R. Soc. Lond. A 337, 165-179.

Brink, H.-J., Burri, P., Lunde, A., Winhard, H., 1992. Hydrocarbon habitat and potential of Swiss and German Molasse Basin: A comparison. Eclogae geol. Helv. 85, 715-732.

Cloetingh, S., 1986. Intraplate stresses: a new tectonic mechanism for relative sea-level fluctuations. Geology 14, 617-620.

Engelder, T., 1993. Stress Regimes in the Lithosphere. Princeton, Princeton University Press, 457 p.

Farr, T.G. et al., 2007. The Shuttle Radar Topography Mission. Rev. Geophys., 45 (RG2004), doi:10.1029/2005RG000183.

Gölke, M., Coblentz, D., 1996. Origins of the European regional stress field. Tectonophysics 266, 11-24.

Grünthal, G., Stromeyer, D., 1986. Stress Pattern in Central Europe and Adjacent Areas. Gerlands Beitr. Geophysik, Leipzig, 95, 443-452.

Grünthal, G., Stromeyer, D., 1992. The recent Crustal Stress Field in Central Europe: Trajectories and Finite Element Modeling. J. Geophys. Res., 97 (B8), 11805-11820.

419 Guzmán, C., Cristallini, E., Bottesi, G., 2007. Contemporary stress orientations in the
420 Andean retroarc between 34ºS and 39ºS from borehole breakout analysis. Tectonics 26,
421 TC3016, doi:10.1029/2006TC001958.

422 Guzmán, C. G., Cristallini, E.O., 2009. Contemporary stress orientations from borehole
423 breakout analysis in the southernmost flat-slab boundary Andean retroarc (32°44' and
424 33°40' S), J. Geophys. Res., 114, B02406, doi:10.1029/2007JB005505.

425 Haimson, B.C., Herrick, C.G., 1989. Borehole breakouts and in situ stress. Proceedings of
426 the 12th Annual Energy Sources Technology Conference, Houston, Texas.

427 Heidbach, O., Reinecker, J., Tingay, M., Müller, B., Sperner, B., Fuchs, K., Wenzel, F.,
428 2007. Plate boundary forces are not enough: Second- and third-order stress patterns
429 highlighted in the World Stress Map database. Tectonics, 26, TC6014
430 doi:10.1029/2007TC002133.

431 Heidbach, O., Tingay, M., Barth, A., Reinecker, J., Kurfeß, D., Müller, B., 2008. The 2008
432 release of the World Stress Map. (available online at www.world-stress-map.org).

433 Heidbach, O., Tingay, M., Barth, A., Reinecker, J., Kurfeß, D., Müller, B., this issue.
434 Global spatial wave-length analysis of the tectonic intraplate stress pattern.
435 Tectonophysics.

436 Heissbauer, H., 1975. Die Gebirgsmechanik beim Abbau in großer Teufe des
437 Kohlebergwerks Peißenberg und ihre Auswirkungen auf die Bergtechnik. Geologica
438 Bavarica 73, 37-53.

439 Hillis, R.R., Holford, S.P., Green, P.F., Doré, A.G., Gatliff, R.W., Stoker, M.S., Thomson,
440 K., Turner, J.P., Underhill, J.R., Williams, G.A., 2008. Cenozoic exhumation of the
441 southern British Isles. Geology 36(5), 371-374.

442 Hubbert, M.K., Willis, D.G., 1957. Mechanics of hydraulic fracturing. AIME Petroleum
443 Transactions 210, 153-166.

444 Huber, K., Schwerd, K., 1995. Das Geologische Profil der Tiefbohrung Hindelang 1
445 (Allgäuer Alpen). Geologica Bavarica 100, 23-54.

446 Illies, J.H., Greiner, G., 1978. Rhinegraben and the Alpine system. GSA Bull. 89, 770-782.

447 Kastrup, U., Zoback, M.L., Deichmann, N., Evans, K.F., Giardini, D., Michael, A.J.,
448 2004. Stress field variations in the Swiss Alps and the northern Alpine foreland derived
449 from inversion of fault plane solutions. J. Geophys. Res. 109, B01402,
450 doi:10.1029/2003JB002550.

451 Kuhlemann, J., Kempf, O., 2002. Post-Eocene evolution of the North Alpine Foreland
452 Basin and its response to Alpine tectonics. Sedimentary Geology 152, 45-78.

453 Mardia, K.V., 1972. Statistics of directional data: probability and mathematical statistics.
454 Academic Press, London, 357 pp.

455 Mastin, L., 1988. Effect of borehole deviation on breakout orientations. J. Geophys. Res.
456 93, 9187-9195.

457 Moos, D., Peska, P., 1998. Predicting the stability of horizontal wells and multilaterals -
458 the role of in situ stress and rock properties. SPE International conference on horizontal
459 well technology.

460 Müller, B., Zoback, M.L., Fuchs, K., Mastin, L., Gregersen, S., Pavoni, N., Stephansson,
461 O., Ljunggren, Ch., 1992. Regional pattern of tectonic stress in Europe. J. Geophys.
462 Res. 97, 11783-11803.

463 Müller, B., Wehrle, V., Zeyen, H., Fuchs, K., 1997. Short-scale variations of tectonic
464 regimes in the western European stress province north of the Alps and Pyrenees.
465 Tectonophysics 275, 199-219.

466 Müller, B., Wehrle, V., Hettel, S., Sperner, B., Fuchs, F., 2003. A new method for
467 smoothing oriented data and its application to stress data. In: M. Ameen (Editor),
468 Fracture and In-situ Stress Characterization of Hydrocarbon Reservoirs. Special
469 Publication. Geological Society, London, pp. 107-126.

470 Müller, M., Nieberding, F., 1995. Die überhydrostatischen Porendrücke in der Bohrung
471 Hindelang 1 (Allgäuer Alpen) und ihre Beziehung zur Umgebung. Geologica Bavarica
472 100, 167-174.

473 Müller, M., Nieberding, F., 1995. Principles of abnormal pressure related to tectonic
474 developments and their implication for drilling activities (Bavarian Alps, Germany). In:
475 G. Wessley and W. Liebl (eds), Oil and gas in Alpidic thrustbelts and basins of Central
476 and Eastern Europe. EAGE special publication, 5, 119-126.

477 Peska, P., Zoback, M.D., 1995. Compressive and tensile failure of inclined wellbores and
478 determination of in situ stress and rock strength. J. of Geophys. Res. 100, 12791-
479 12811.

480 Plumb, R.A., Hickman, S.H., 1985. Stress-induced borehole elongation: a comparison
481 between the four-arm dipmeter and the borehole televiewer in the Auburn geothermal
482 well. J. Geophys. Res. 90, 5513-5521.

483 Reinecker, J., Lenhardt, W.A., 1999. Present-day stress field and deformation in Eastern
484 Austria. Int. Journ. Earth Sciences, 88, 532-550.

485 Reinecker, J., Tingay, M., Müller, B., 2003. Borehole breakout analysis from four-arm
486 caliper logs. World Stress Map Project Stress Analysis Guidelines (available online at
487 www.world-stress-map.org).

488 Reinecker, J., Heidbach, O., Tingay, M., Sperner, B., Müller, B., 2005. The 2005 release of
489 the World Stress Map.

490 Richardson, R.M., 1992. .Ridge forces, absolute plate motions, and the intraplate stress
491 field. Journal of Geophysical Research, 97, 11739-11748.

492 Schrader, F., 1988. Das regionale Gefüge der Drucklösungsdeformation an Geröllen im
493 westlichen Molassebecken. Geol. Rdsch. 77, 347-369.

494 Sibson, R.H., 1996. Structural permeability of fluid-driven fault-fracture meshes. J. of
495 Struct.l Geo. 18, 1031-1042.

496 Sonder, L.J., 1990. Effects of density contrasts on the orientation of stresses in the
497 lithosphere: relation to principal stress direction in the Transverse Ranges, California.
498 Tectonics 9(4), 761-771.

499 Tingay, M., Müller, B., Reinecker, J., Heidbach, O., 2006. State and origin of the present-
500 day stress field in sedimentary basins: New results from the World Stress Map project.
501 41st U.S. Rock Mech. Symp., Golden Rocks 2006, Golden/Colorado, 17.-21.6.2006,
502 published plenary paper ARMA/USRMS 06-1049.

503 Tingay, M., Reinecker, J., Müller, B., 2008. Borehole breakout and drilling-induced
504 fracture analysis from image logs. World Stress Map Project Stress Analysis
505 Guidelines (available online at www.world-stress-map.org).

506 Trümpy, R., 1980. Geology of Switzerland, Part A: An Outline of the Geology of
507 Switzerland. 104 p., Wepf & Co. Publishers (Basel).

508 Zajak, B.J., Stock, J.M., 1997. Using borehole breakouts to constrain the complete stress
509 tensor: Results from the Siljan Deep Drilling Project and offshore Santa Maria Basin,
510 California. J. Geophys. Res. 102, 10083-10100.

511 Ziegler, P.A., 1987. Late Cretaceous and Cenozoic intra-plate compressional deformations
512 in the Alpine foreland – a geodynamic model. Tectonophysics 137, 389-420.

513 Ziegler, P.A., 1990. Geological Atlas of Western and Central Europe 1990. Shell
514 Internationale Petroleum Maatschappij, Den Haag, The Netherlands, 239 p.

515 Zoback, M.D., Moos, D., Mastin, L.G., Anderson, R.N., 1985. wellbore breakouts and in
516 situ stress. J. of Geophys. Res. 90, 5523-5530.

517 Zoback, M.L., 1992. First- and second-order patterns of stress in the lithosphere: The
518 world stress map project. J. of Geophys. Res. 97, 11703-11728.

519 Zoback, M.L., Mooney, W.D., 2003. Lithospheric buoyancy and continental intraplate
520 stresses. Int. Geology Rev. 45, 95-118.

521

522

523 **Figure captions**

524 **Figure 1. (A)** Overview of the Swiss-German Molasse Basin with contour lines of the base
525 of Tertiary sediments (i.e. the Molasse sediments) and major structures **(B)** N-S profile
526 through the German Molasse Basin.

527

528 **Figure 2.** Present-day orientation of maximum horizontal stress (S_H) determined in this
529 study from borehole breakouts and drilling-induced fractures. Symbol size is proportional
530 to quality of the data. Names identify the wellbore locations according to Table 1. **(A)** A-D
531 quality stress orientations (long axes of symbols) in 96 wells across the German Molasse
532 Basin demonstrate that the present-day S_H in the German Molasse Basin is predominantly
533 oriented N-S. However, localized stress perturbations are observed in Hindelang,
534 Illmensee, Mönchsrot, Tacherting and Vorderiss. **(B)** Detailed view of stress orientations in
535 southeast Germany (same legend as in A). Topography data are from the SRTM project
536 (Farr et al., 2007). **(C)** Rose diagram of the S_H orientations from Fig. 2a. Petal length
537 represents the relative number of wells clustered in 10° azimuthal bins. The overall mean
538 of the maximum horizontal stress orientation ($\overline{S}_H$) and standard deviation (s.d.) for each
539 dataset was calculated using the Mardia statistics for bi-polar data (Mardia, 1972). Note
540 that the standard deviation significantly decreases when D-quality data are omitted.

541

542 **Figure 3.** Occurrence of stress induced borehole failure in the German Molasse Basin with
543 depth, S_H orientation, and level of differential stress depending on **(A and B)** latitude and
544 **(C and D)** longitude. Occurrence with depth is indicated by the vertical bars. The quality
545 of S_H orientation is color coded (see inset). Ratio of BO length to log length as a proxy for
546 differential stress is generally high. There is no significant stress rotation with depth within
547 the entire Molasse Basin. Also there is no significant change in stress down into the pre-

548 Tertiary basement. The labeled wells are further discussed in the text. Note that the thick
549 grey dashed lines give only a rough orientation for the base of Tertiary and the front of
550 Alpine nappes. Both vary along strike of the Alpine front. The base of Tertiary is up to 3
551 km higher in the western German Molasse basin than indicated in (A). Here a
552 representative depth is given for the eastern part (comparable to the profile given in Figure
553 1), where most well bores are located.
554
555 **Figure 4.** Present-day S_H orientations in the Molasse Basin from the analysis herein and
556 from the 2005 World Stress Map database (Reinecker et al., 2005). S_H rotates from N-S in
557 the Eastern Alps (000ºN ± 23º) to NNW-SSE in the Western Alps (150ºN ± 24º). Legends
558 for rose diagrams are the same as in Fig.2. The S_H orientation is roughly perpendicular to
559 the topographic front throughout the basin, indicating that forces originating from the
560 gravitational potential energy of the Alps (rather than plate boundary forces) are
561 controlling the Molasse Basin stress field. See inset legend for details on data types, stress
562 regime (NF = normal faulting, SS = strike-slip, TF = thrust faulting, U = undefined), and
563 quality ranking. Thin black lines are the trajectories of maximum horizontal stress
564 calculated using a quality and distance weighted approach with a smoothing radius of
565 100 km (as described in Müller et al., 2003).
566
567 **Table Captions**
568 **Table 1.** Summary of breakout and drilling-induced fracture analysis results from 132
569 wells in the German Molasse Basin sorted by longitude. S_H = average maximum horizontal
570 stress orientation (ºN). # = number of breakouts (BO) or drilling-induced fractures (DIF),
571 s.d. = standard deviation, total = total length of BO/DIF, top and bottom =

572 shallowest/deepest BO/DIF observed in well. Data are included in World Stress Map 2008

573 database release (Heidbach et al, 2008).

Figure_01

Click here to download high resolution image

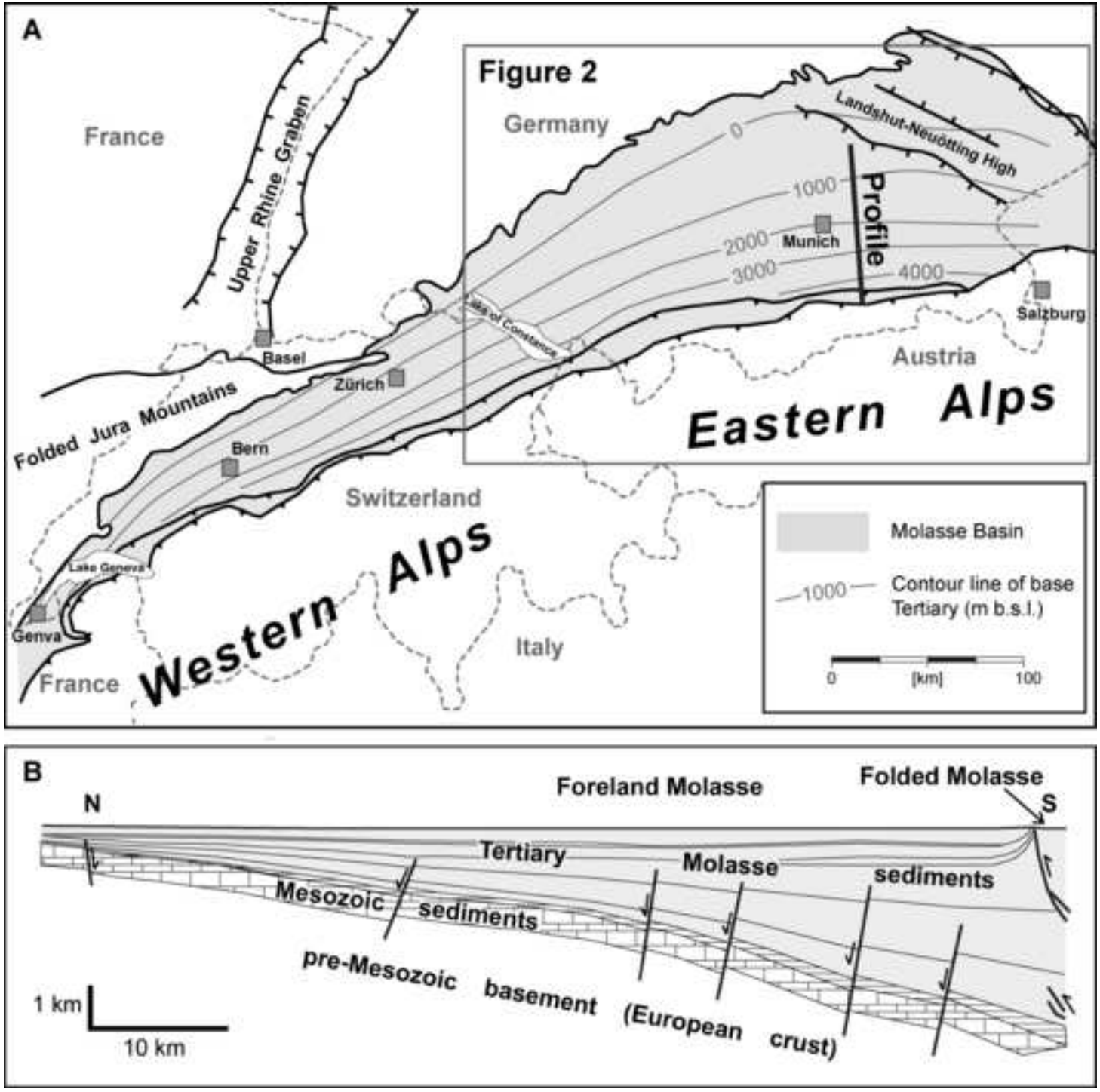

Figure_02

Click here to download high resolution image

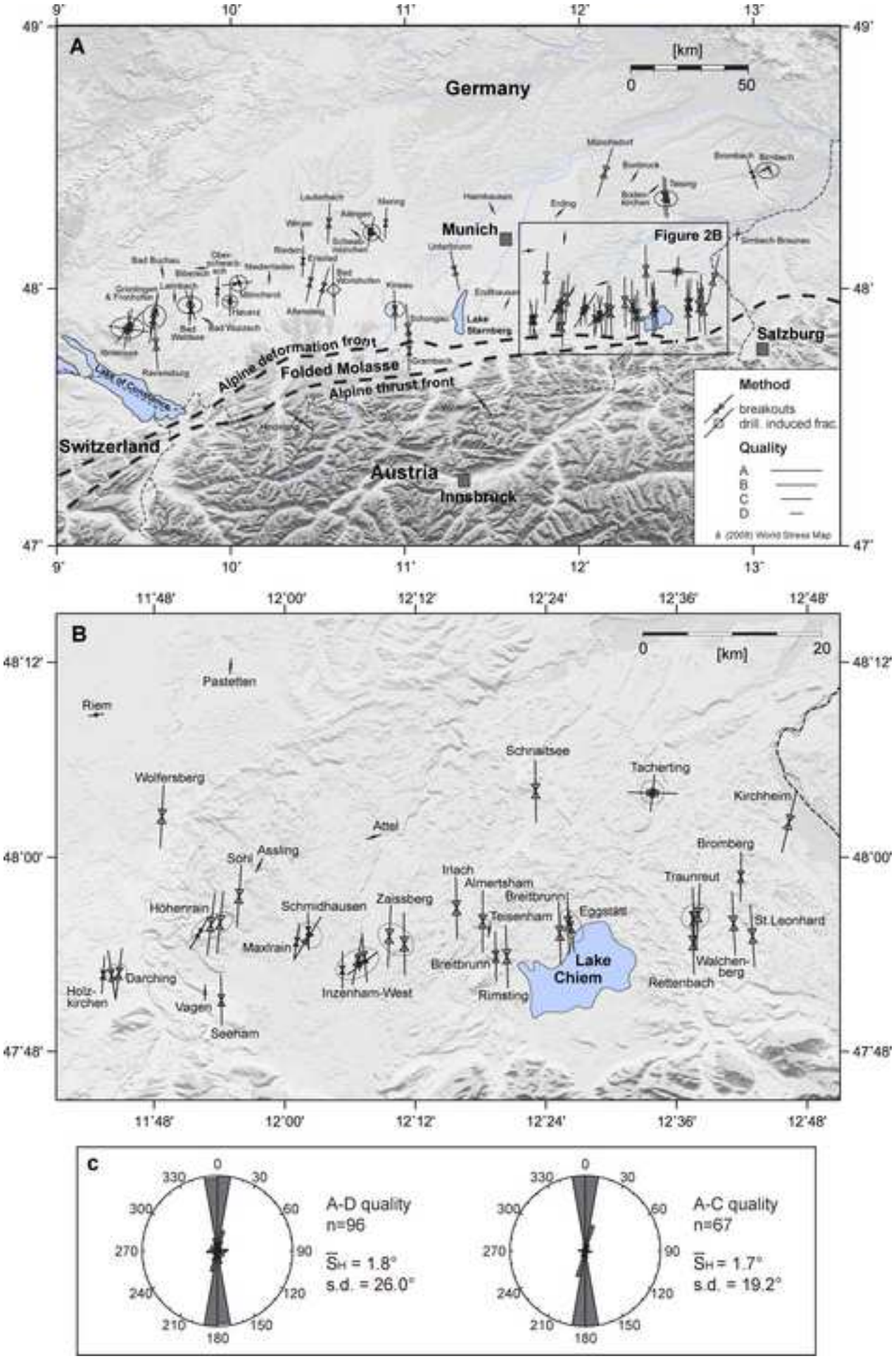

Figure_03

Click here to download high resolution image

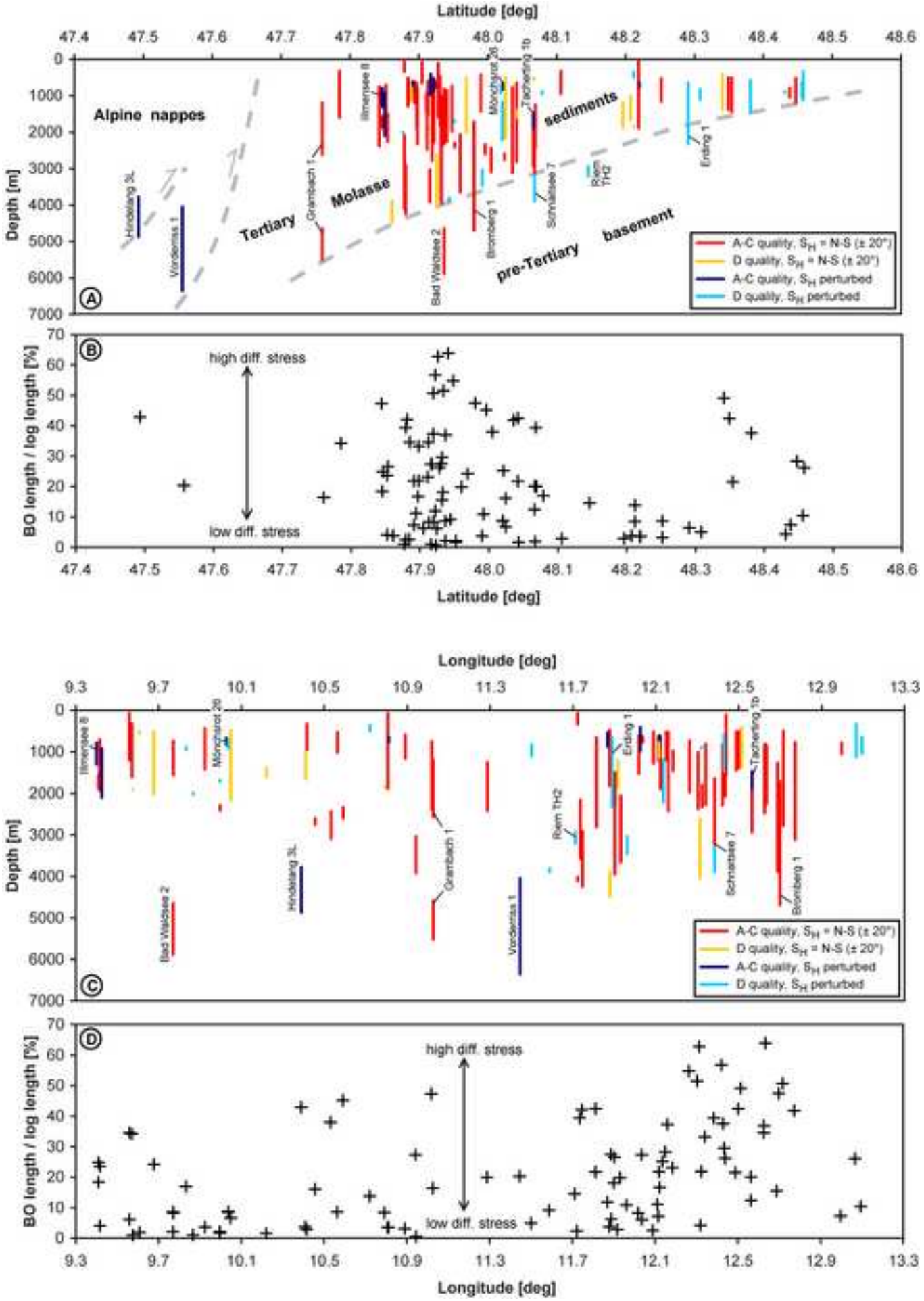

Figure_04

Click here to download high resolution image

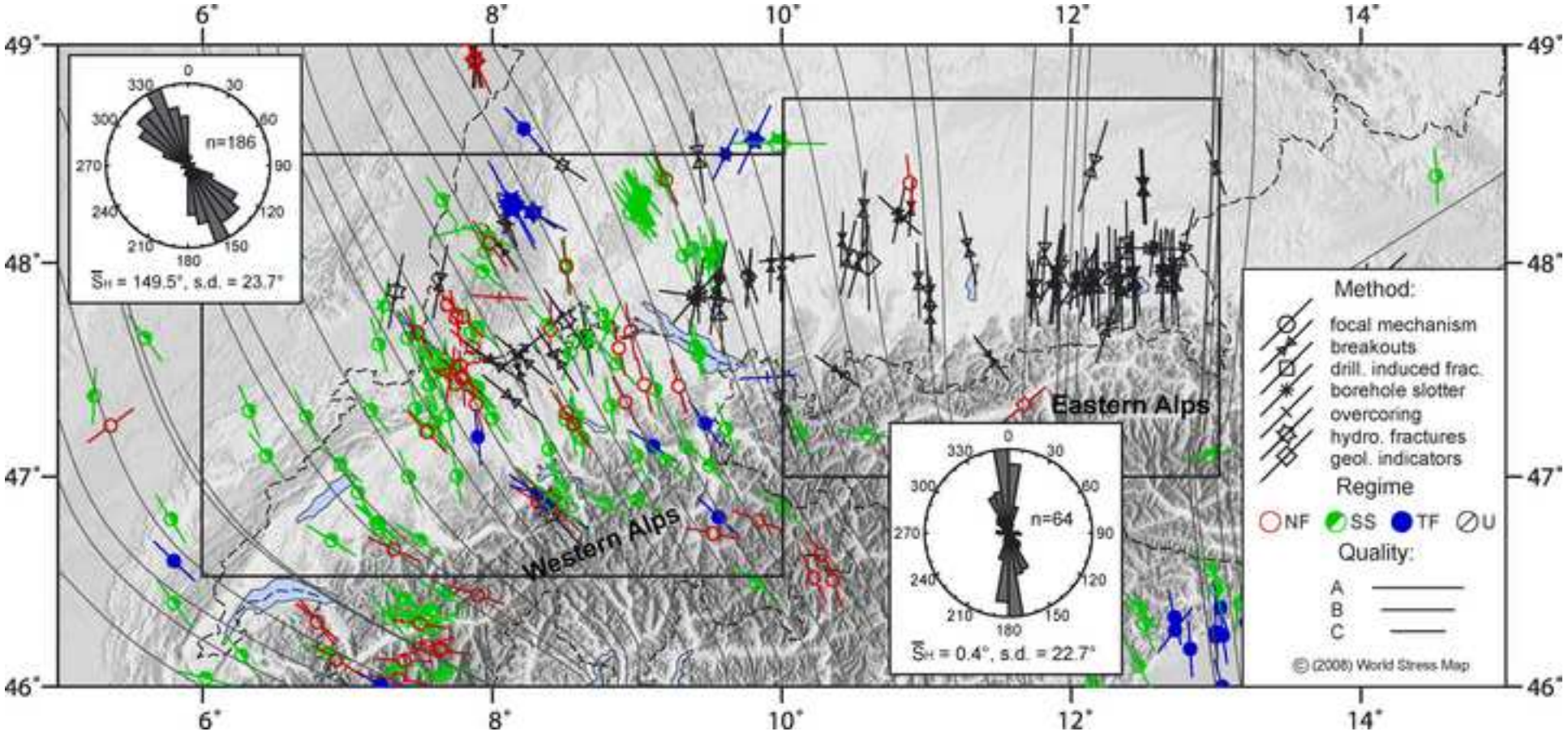

Table_01

Click here to download Table: Table_1_final.doc

Table 1.

lat	long	S_H	Type	Depth [km]	Quality	Locality	#	s.d.	Total [m]	Top [m]	Bottom [m]
47.846	9.41	11	BO	1.7	B	Illmensee 7	4	9	169	1558	1878
47.845	9.41	98	BO	1.0	B	Illmensee 8	9	7	170	785	1304
47.852	9.416	40	BO	1.5	B	Illmensee 5	8	20	364	916	2099
47.852	9.416	177	BO	1.3	C	Illmensee 6	12	16	66	703	1930
47.885	9.559	10	BO	0.9	A	Grünlingen 1	38	11	344	518	1200
47.905	9.559	11	BO	0.4	B	Fronhofen 16	9	10	111	74	645
47.785	9.571	176	BO	1.0	A	Ravensburg 1	19	7	490	319	1598
47.916	9.575	165	BO	1.9	D	Fronhofen 23	1	-	5	1904	1908
48.067	9.607	172	BO	0.5	D	Bad Buchau	2	10	10	508	554
47.969	9.677	177	BO	1.3	D	Laimbach 1	30	27	296	510	2021
47.937	9.769	5	DIF	5.1	C	Bad Waldsee 2	7	16	31	4641	5563
47.937	9.769	161	BO	5.3	C	Bad Waldsee 2	25	20	123	4674	5879
47.919	9.771	5	BO	1.1	C	Bad Waldsee 1	6	5	79	737	1556
48.079	9.832	87	BO	0.9	D	Jordanbad Biberach 1	2	10	30	887	945
47.877	9.866	121	BO	2.0	D	Bad Wurzach 3	3	7	15	1993	2018
47.99	9.924	2	BO	0.9	C	Oberschwarzach 4	4	7	45	426	1420
47.99	9.932	-	BO	-	E	Oberschwarzach 3	-	-	-	-	-
47.952	9.996	100	BO	1.7	D	Hauerz 3	1	-	32	1680	1712
47.952	9.997	2	BO	2.3	C	Hauerz 1	5	2	33	2288	2411
47.953	10.011	-	BO	-	E	Hauerz 2	-	-	-	-	-
48.02	10.036	83	BO	0.7	C	Mönchsrot 26	12	15	97	664	829
48.02	10.036	81	BO	0.8	D	Mönchsrot 26A	8	32	76	690	916
48.024	10.048	161	BO	1.3	D	Mönchsrot 27	13	37	126	485	2171
48.224	10.172	-	BO	-	E	Buch 1	-	-	-	-	-
48.043	10.22	0	BO	1.5	D	Niederrieden 1	2	0	5	1383	1599
48.061	10.246	-	BO	-	E	Lauberhart 3	-	-	-	-	-
48.061	10.246	-	BO	-	E	Lauberhart 1	-	-	-	-	-
48.071	10.248	-	BO	-	E	Lauberhart 2	-	-	-	-	-
48.112	10.365	-	BO	-	E	Arlesried 11	-	-	-	-	-
48.113	10.38	-	BO	-	E	Arlesried 29	14	46	405	423	1337
47.493	10.389	125	BO	4.3	C	Hindelang 3L	15	22	505	3778	4866
48.207	10.409	175	BO	1.3	D	Winzer 1	2	0	56	1012	1653
48.106	10.415	2	BO	0.6	C	Rieden 3	8	3	33	323	947
48.024	10.456	11	BO	2.7	B	Erisried 1	4	2	121	2597	2748
48.005	10.531	16	BO	2.7	B	Altensteig 1	10	17	288	2435	3090
48.252	10.563	3	BO	0.7	B	Lauterbach 1	14	7	102	526	1010
47.996	10.591	178	DIF	2.4	A	GT2 Bad Worishofen	22	6	122	2337	2596
48.152	10.602	-	BO	-	E	Zaisertshofen 5	-	-	-		
48.212	10.721	130	BO	0.4	D	Schwabmünchen 4	2	26	135	355	497
48.212	10.791	174	BO	1.85	D	Aitingen 1	2	2	6	1843	1859
48.218	10.795	-	BO	-	E	Aitingen 5	-	-	-	-	-
48.221	10.8	-	BO	-	E	Aitingen 6	-	-	-	-	-
48.219	10.806	12	BO	1.0	C	Aitingen 2	18	10	70	67	1890
48.22	10.812	132	BO	0.7	C	Aitingen 4a	4	15	26	647	760
48.22	10.812	-	BO	-	E	Aitingen 4	-	-	-	-	-
48.252	10.89	3	BO	0.9	C	Mering 1	8	8	40	591	1157
47.91	10.923	-	BO	-	E	Kinsau 2	-	-	-	-	-
47.916	10.942	178	BO	3.4	B	Kinsau 1	8	7	250	3035	3916
47.923	10.945	165	BO	3.2	D	Kinsau 3	1	-	2	3224	3226
47.844	11.018	176	BO	1.5	A	Schongau 1	39	8	828	752	2382
47.76	11.025	1	BO	3.3	B	Grambach 1	52	17	711	1192	5509
48.069	11.287	167	BO	1.8	B	Unterbrunn 3	9	4	354	1248	2418
48.286	11.442	-	DIF	-	E	Hebertshausen 4a	2	0	1	1555	1565
48.286	11.442	-	BO	-	E	Hebertshausen 1	-	-	-	-	-
47.557	11.445	142	BO	5.1	C	Vorderriss 1	60	27	490	4043	6353
48.308	11.5	155	BO	0.9	D	Haimhausen 1 and 1a	2	0	52	822	1097
48.312	11.531	-	BO	-	E	Haimhausen 2	-	-	-	-	-
47.944	11.587	24	BO	3.8	D	Endlhausen 1	5	11	23	3808	3887
48.146	11.711	81	DIF	3.1	D	Riem TH2	18	40	44	2935	3206
47.879	11.722	4	BO	2.0	C	Holzkirchen 3	6	11	66	71	4107
47.879	11.735	171	BO	3.1	B	Darching 5	16	14	970	2155	3575
47.881	11.746	7	BO	3.6	B	Darching 3	31	21	1017	2910	4240
48.042	11.812	3	BO	1.7	A	Wolfersberg 11	42	7	1002	653	2812
48.042	11.812	3	BO	1.3	A	Wolfersberg 10a	18	3	517	695	1927
48.042	11.812	35	BO	1.2	E	Wolfersberg 9	37	48	321	700	1802
48.105	11.813	-	BO	-	E	Poering 1	-	-	-	-	-
47.796	11.839	-	BO	-	E	Miesbach 1	-	-	-	-	-
47.922	11.869	30	BO	0.7	C	Höhenrain A5	4	17	166	535	868
47.922	11.869	-	BO	-	E	Höhenrain H1	-	-	-	-	-
47.861	11.878	0	BO	4.2	D	Vagen 1	2	0	40	3890	4478
47.931	11.887	7	BO	1.2	A	Höhenrain 4	20	4	541	470	1822
48.291	11.888	43	BO	1.5	D	Erding 1	22	40	114	644	2323
47.933	11.901	6	BO	2.8	A	Höhenrain 6	27	8	366	1962	3950
47.853	11.903	179	BO	1.8	B	Seeham C1	9	3	432	1491	2260

48.196	11.917	4	BO	1.5	D	Pastetten 1	3	4	31	1201	1864
47.96	11.93	4	BO	2.8	A	Söhl 1	13	4	413	2057	3648
47.992	11.961	25	BO	3.2	D	Assling 5	7	27	199	3037	3460
47.992	11.961	-	BO	-	E	Assling 5a	-	-	-	-	-
47.913	12.018	8	BO	1.0	C	Maxlrain A1	6	4	94	606	1518
47.917	12.035	32	BO	0.7	B	Schmidhausen A3	7	5	166	403	970
47.924	12.036	179	BO	0.7	C	Schmidhausen A2	8	3	40	629	768
47.919	12.068	-	BO	-	E	Schmidhausen-Ost C1	-	-	-	-	-
47.884	12.088	0	BO	0.8	C	Inzenham-West 3	13	7	27	518	1280
48.33	12.089	-	BO	-	E	Hofkirchen 2	-	-	-	-	-
47.893	12.092	-	BO	-	E	Inzenham-West 2	-	-	-	-	-
47.892	12.105	108	BO	0.8	E	Inzenham-West 11	2	3	68	645	923
47.894	12.111	11	BO	1.0	B	Inzenham-West 4	12	3	94	620	1198
47.886	12.112	-	BO	-	E	Inzenham-West 42	-	-	-	-	-
47.891	12.115	4	BO	1.0	D	Inzenham-West 23	3	7	58	775	1145
47.891	12.119	52	BO	0.7	C	Inzenham-West 14	12	11	73	608	866
47.897	12.122	174	BO	1.2	B	Inzenham-West C5	11	6	223	656	1892
48.021	12.136	73	BO	1.7	D	Attel 3	13	43	303	1180	2213
48.447	12.149	17	BO	0.8	A	Münchsdorf 1	18	8	314	519	1191
47.919	12.16	3	BO	1.5	A	Zaissberg C4	14	5	926	525	2420
47.911	12.183	179	BO	1.2	A	Zaissberg C3	18	4	231	970	1450
47.948	12.263	179	BO	1.3	A	Irlach C1	11	2	704	731	1966
47.929	12.298	-	BO	-	E	Almertsham C2	-	-	-	-	-
47.934	12.303	0	BO	1.7	A	Almertsham C1	32	4	755	1010	2375
47.926	12.313	7	BO	3.3	D	Teisenham 1	16	32	925	2602	4044
48.431	12.319	30	BO	0.9	D	Bonbruck 2	1	-	23	887	910
47.898	12.323	179	BO	2.1	B	Breitbrunn C4	16	3	151	1800	2328
47.898	12.34	178	BO	1.5	A	Rimsting C1	15	12	494	814	2273
47.91	12.358	-	BO	-	E	Breitbrunn C5	-	-	-	-	-
48.068	12.384	1	BO	2.2	A	Schnaitsee 7	14	8	926	1640	2793
48.068	12.384	147	BO	3.8	D	Schnaitsee 7	2	3	58	3733	3869
47.912	12.407	-	BO	-	E	Breitbrunn C1	-	-	-	-	-
47.922	12.421	178	BO	1.5	A	Breitbrunn C10	24	5	1020	834	2286
47.928	12.426	-	BO	-	E	Eggstätt C1	-	-	-	-	-
48.381	12.428	48	BO	1	D	Bodenkirchen 1 - 1a	15	46	454	575	1463
47.932	12.434	178	BO	1.5	A	Eggstätt C2	19	10	341	1325	2066
47.923	12.435	-	BO	-	E	Breitbrunn 22	-	-	-	-	-
47.923	12.435	-	BO	-	E	Breitbrunn 21	-	-	-	-	-
47.923	12.435	-	BO	-	E	Breitbrunn 26	-	-	-	-	-
47.923	12.435	-	BO	-	E	Breitbrunn C6	-	-	-	-	-
47.928	12.438	172	BO	1.0	B	Eggstätt C4	17	13	249	105	1583
48.354	12.488	177	BO	0.9	B	Teising 1	10	4	167	507	1442
48.349	12.502	177	BO	0.9	B	Teising 2	12	19	456	506	1381
48.341	12.514	172	BO	0.9	D	Teising 3	19	35	512	412	1376
47.9	12.544	-	BO	-	E	Chieming C1	-	-	-	-	-
48.066	12.563	91	BO	1.6	B	Tacherting 1-b	5	2	259	1465	1890
48.066	12.563	6	BO	2.4	C	Tacherting 1-a	2	6	419	1900	2936
48.141	12.585	-	BO	-	E	Garching 1	-	-	-	-	-
47.912	12.625	178	BO	1.7	A	Rettenbach C2	27	6	635	887	2478
47.937	12.626	178	BO	1.6	A	Traunreut A3	25	4	591	814	2321
47.941	12.633	3	BO	1.5	A	Traunreut A2	21	4	1185	852	2258
48.158	12.641	-	BO	-	E	Hinterberg 2	-	-	-	-	-
47.985	12.649	-	BO	-	E	Traunreut C1	-	-	-	-	-
47.932	12.687	177	BO	2.5	A	Walchenberg 1	11	8	397	1269	3878
47.98	12.698	1	BO	3.2	B	Bromberg 1	54	20	1716	1713	4690
48.177	12.704	-	BO	-	E	Pirach 1	-	-	-	-	-
47.919	12.716	176	BO	1.6	A	St.Leonhard C1	31	4	1435	492	2778
48.036	12.772	13	BO	2.4	A	Kirchheim C1	27	6	1017	768	3112
48.338	12.777	-	BO	-	E	Wurmannsquick 1	-	-	-	-	-
48.299	12.965	-	BO	-	E	Taubenbach 1	-	-	-	-	-
48.438	12.996	160	BO	0.9	C	Brombach 1	15	11	69	783	1044
48.258	13.01	5	DIF	1.8	D	Simbach-Braunau TH1	10	8	11	1770	1839
48.458	13.067	60	BO	0.7	D	Birnbach 5	16	41	265	328	1127
48.456	13.094	152	BO	0.8	D	Birnbach T 4	7	32	71	648	1042